Competition among Nasal Bacteria Suggests a Role for Siderophore-Mediated Interactions in Shaping the Human Nasal Microbiota

Reed M. Stubbendieck,[a] Daniel S. May,[a] Marc G. Chevrette,[a,b] Mia I. Temkin,[a] Evelyn Wendt-Pienkowski,[a] Julian Cagnazzo,[a] Caitlin M. Carlson,[a] James E. Gern,[c,d] Cameron R. Currie[a]

[a]Department of Bacteriology, University of Wisconsin—Madison, Madison, Wisconsin, USA
[b]Laboratory of Genetics, University of Wisconsin—Madison, Madison, Wisconsin, USA
[c]Department of Pediatrics, University of Wisconsin School of Medicine and Public Health, Madison, Wisconsin, USA
[d]Department of Medicine, University of Wisconsin School of Medicine and Public Health, Madison, Wisconsin, USA

ABSTRACT Resources available in the human nasal cavity are limited. Therefore, to successfully colonize the nasal cavity, bacteria must compete for scarce nutrients. Competition may occur directly through interference (e.g., antibiotics) or indirectly by nutrient sequestration. To investigate the nature of nasal bacterial competition, we performed coculture inhibition assays between nasal *Actinobacteria* and *Staphylococcus* spp. We found that isolates of coagulase-negative staphylococci (CoNS) were sensitive to growth inhibition by *Actinobacteria* but that *Staphylococcus aureus* isolates were resistant to inhibition. Among *Actinobacteria*, we observed that *Corynebacterium* spp. were variable in their ability to inhibit CoNS. We sequenced the genomes of 10 *Corynebacterium* species isolates, including 3 *Corynebacterium propinquum* isolates that strongly inhibited CoNS and 7 other *Corynebacterium* species isolates that only weakly inhibited CoNS. Using a comparative genomics approach, we found that the *C. propinquum* genomes were enriched in genes for iron acquisition and harbored a biosynthetic gene cluster (BGC) for siderophore production, absent in the noninhibitory *Corynebacterium* species genomes. Using a chrome azurol S assay, we confirmed that *C. propinquum* produced siderophores. We demonstrated that iron supplementation rescued CoNS from inhibition by *C. propinquum*, suggesting that inhibition was due to iron restriction through siderophore production. Through comparative metabolomics and molecular networking, we identified the siderophore produced by *C. propinquum* as dehydroxynocardamine. Finally, we confirmed that the dehydroxynocardamine BGC is expressed *in vivo* by analyzing human nasal metatranscriptomes from the NIH Human Microbiome Project. Together, our results suggest that bacteria produce siderophores to compete for limited available iron in the nasal cavity and improve their fitness.

IMPORTANCE Within the nasal cavity, interference competition through antimicrobial production is prevalent. For instance, nasal *Staphylococcus* species strains can inhibit the growth of other bacteria through the production of nonribosomal peptides and ribosomally synthesized and posttranslationally modified peptides. In contrast, bacteria engaging in exploitation competition modify the external environment to prevent competitors from growing, usually by hindering access to or depleting essential nutrients. As the nasal cavity is a nutrient-limited environment, we hypothesized that exploitation competition occurs in this system. We determined that *Corynebacterium propinquum* produces an iron-chelating siderophore, and this iron-sequestering molecule correlates with the ability to inhibit the growth of coagulase-negative staphylococci. Furthermore, we found that the genes required for siderophore production are expressed *in vivo*. Thus, although siderophore production by

bacteria is often considered a virulence trait, our work indicates that bacteria may produce siderophores to compete for limited iron in the human nasal cavity.

Humans engage in symbioses with diverse sets of microbes at nearly every body site. Collectively, these microbes are referred to as the human microbiota. Members of the microbiota provide their human host with essential services. For example, within the gastrointestinal tract, mutualistic bacteria metabolize recalcitrant nutrients to release metabolites that are accessible to the human host (1, 2); synthesize many essential amino acids, cofactors, and vitamins (3, 4); and provide defense against pathogens (5, 6). However, despite providing critical services to their hosts, nutrient acquisition is often a principal challenge for bacteria colonizing humans and other animals. In part, this is due to host sequestration of resources as a means to control bacterial growth (7).

To form and maintain associations with humans and other eukaryotes, bacteria have evolved mechanisms to derive nutrition from their hosts (8, 9). Both commensal and pathogenic bacteria colonizing the gastrointestinal tract consume host-derived compounds (10). For instance, *Bacteroides acidifaciens* and *Akkermansia muciniphila* cells have been shown to incorporate carbon and nitrogen from host proteins (11), and the pathogen *Salmonella enterica* serotype Typhimurium uses tetrathionate derived from thiosulfate that is produced by the host inflammatory response during infection as a terminal electron acceptor (12). In addition to consuming host-derived products, bacteria colonizing the gastrointestinal tract can also acquire nutrients from meals that their host consumes (10). However, outside the gastrointestinal tract, bacteria have increasingly limited access to nutrients. *Cutibacterium* (*Propionibacterium*) *acnes* colonizing the sebaceous glands in human skin hydrolyzes sebum triglycerides to generate free fatty acids and glycerol (13, 14), which it may metabolize (15). Similarly, anaerobic oral bacteria that have spread to the lower respiratory tracts of cystic fibrosis patients may ferment host mucins to generate short-chain fatty acids and amino acids to feed other bacteria, including *Pseudomonas aeruginosa* (16).

To colonize the upper airway, bacteria must attach to the epithelial surface, accommodate or evade the host's immune system, and cope with decreased access to freely available nutrients compared to bacteria colonizing the gastrointestinal tract (reviewed in reference 7). Within the human nasal cavity, there are minute concentrations of free amino acids, carbohydrates, organic acids, and minerals (17–19). For comparison, nasal secretions contain ~65-fold-lower glucose concentrations than the lumen of the small intestine (19, 20). Furthermore, humans actively deplete the available glucose in the airway through polarized glucose importers in the membranes of airway epithelial cells (21). Similar to other environments such as the soil or the ocean, the bioavailability of iron in the nasopharynx is low (17, 18). As a means to acquire scarce iron, bacteria and other microbes release iron-chelating molecules called siderophores that can scavenge ferric iron and other minerals from the environment (22). However, human hosts have evolved countermeasures to circumvent bacterial siderophores. For instance, bacterial colonization of the nasopharynx triggers neutrophils to produce lipocalin-2, a protein that binds to enterobactin-type siderophores and prevents their uptake by bacteria (23, 24). Finally, in addition to experiencing nutrient and mineral limitation, bacteria that colonize the nasal cavity are exposed to oxygen stress, which may be either abiotic or produced by the action of host immune cells (25, 26). Therefore, the human nasal cavity is a low-resource and high-stress environment, requiring bacteria in this environment to engage in competitive interactions for survival (27, 28).

Competition is split into two modes, called interference and exploitation. Bacteria engaging in exploitation competition compete by preventing their competitors from accessing resources, by either rapidly consuming or sequestering these supplies. In contrast, bacteria using interference competition produce toxic effectors to directly

inhibit their competitors (29). Bacteria isolated from the human nasal cavity are well known to use specialized (secondary) metabolites with antimicrobial properties to engage in interference competition. As examples, *Staphylococcus lugdunensis* produces a thiazolidine-containing cyclic peptide called lugdunin that inhibits the growth of *Staphylococcus aureus in vitro*. In a patient population, nasal colonization by *S. lugdunensis* was significantly associated with decreased *S. aureus* colonization, suggesting that lugdunin is produced *in vivo* (30). Similarly, *Corynebacterium accolens* secretes a lipase that cleaves human nasal triacylglycerols to produce antimicrobial free fatty acids that inhibit the growth of *Streptococcus pneumoniae in vitro*. In a 16S rRNA gene amplicon sequencing survey, the abundance of *Corynebacterium* species sequencing reads was increased in children negative for pneumococcal colonization, indicating that *C. accolens* may inhibit *S. pneumoniae in vivo* (31). Finally, under conditions of iron limitation and hydrogen peroxide-induced oxidative stress, which reflect conditions experienced by bacteria colonizing the nasal cavity, *Staphylococcus epidermidis* IVK45 increases the production of an antimicrobial peptide called nukacin IVK45 *in vitro* (32). Despite these examples of interference competition and the low-resource environment of the nasal cavity, mechanisms of exploitation competition are not well studied among members of the human nasal microbiota (33).

In this study, we investigated bacterial competition between *Actinobacteria* and *Staphylococcus*, which are among the most abundant members of the human nasal microbiota (33, 34). We found that *Corynebacterium* (phylum *Actinobacteria*) strains vary in their ability to inhibit the growth of coagulase-negative staphylococci (CoNS). Using a comparative genomics approach, we identified a gene cluster for siderophore biosynthesis that is present in the genomes of *Corynebacterium propinquum* strains that more strongly inhibit CoNS. We confirmed siderophore production and demonstrated that iron sequestration was the mechanism of CoNS inhibition. We identified the siderophore as dehydroxynocardamine. Finally, we detected the expression of the dehydroxynocardamine biosynthetic gene cluster (BGC) in metatranscriptomic reads from the human nasal cavity. Together, the data suggest that members of the human nasal microbiota engage in exploitation competition for limiting iron and may influence the composition of the human nasal microbiota *in vivo*.

RESULTS

Interaction assays reveal variation in staphylococcal inhibition by nasal *Actinobacteria*. The scarcity of nutrients and minerals in the human nasal cavity results in a stressful environment where the microbiota must compete to survive. To identify mechanisms of competition that occur among members of the nasal microbiota, we chose to use a culture-based approach and investigated interactions between *Actinobacteria* and *Staphylococcus* spp., which are major bacterial colonizers of the human nasal cavity. For this study, we isolated bacteria from frozen nasal lavage samples donated by healthy children as part of the Childhood Origins of Asthma (COAST) study (35, 36), which we identified by colony morphology, pigmentation, hemolysis, and 16S rRNA gene sequence (see Materials and Methods).

To identify differences in patterns among interactions between *Actinobacteria* and *Staphylococcus* spp., we assessed the ability of a subset of *Actinobacteria* isolates to inhibit the growth of a subset of *Staphylococcus* species isolates. In total, we tested 21 *Actinobacteria* isolates (10 *Corynebacterium*, 1 *Curtobacterium*, 1 *Dermabacter*, 3 *Kocuria*, 1 *Microbacterium*, 3 *Micrococcus*, and 2 *Rothia* isolates) against 39 *Staphylococcus* species isolates (15 *S. aureus* isolates, 5 *Staphylococcus warneri/S. pasteuri* isolates, and 19 other CoNS) (see Table S1 in the supplemental material), for a total of 812 pairwise combinations with ≥2 replicates. In the case of 7 combinations, the replicates were not in agreement, or the *Actinobacteria* isolate overgrew its well and prohibited inoculation of the *Staphylococcus* species isolate. We removed these 7 points from further analysis. We scored inhibition by visual inspection of the *Staphylococcus* species colonies after 1 week of coincubation. Strong inhibition corresponded to colonies with severe growth defects or total growth inhibition, whereas weak inhibition corresponded to colonies

with moderate inhibition resulting in diminished growth. *Staphylococcus* species colonies that were indistinguishable from a monoculture control were considered uninhibited (Fig. 1A). To visualize patterns in the inhibition assays, we plotted the inhibition scores as a heat map that was clustered based on the phylogenetic relationships of the *Actinobacteria* and *Staphylococcus* species isolates on the horizontal and vertical dimensions, respectively. The *Staphylococcus* species phylogenetic tree was built from 16S rRNA gene sequence alignments, whereas the *Actinobacteria* phylogenetic species tree was built from alignments of 93 single-copy core bacterial genes (Fig. 1B).

By clustering the inhibition scores with respect to phylogeny, we immediately observed significant differences in the inhibition patterns between *S. aureus* and CoNS. Broadly, most CoNS isolates were inhibited by nasal *Actinobacteria*, but the *S. aureus* isolates were insensitive ($\chi^2 = 371.73$; $df = 2$; $P < 2.2e-16$) (Fig. 1B). However, the inhibition pattern was not solely dominated by the identity of the *Staphylococcus* species; we observed variation among *Corynebacterium* species isolates in inhibiting CoNS. In particular, we noticed three *Corynebacterium* species isolates forming a monophyletic clade (highlighted in orange in Fig. 1B) that more strongly inhibited the growth of CoNS than the other *Corynebacterium* species isolates ($\chi^2 = 89.74$; $df = 2$; $P < 2.2e-16$) (Fig. 1B). Given the limited variation in staphylococcal inhibition scores by other genera of *Actinobacteria*, we focused on *Corynebacterium* spp. to determine underlying factors responsible for the differences between weak and strong CoNS inhibitors.

Corynebacterium propinquum strongly inhibits CoNS. To identify the *Corynebacterium* strains, we constructed a core-genome phylogeny from the 10 *Corynebacterium* spp. that we isolated and 45 human-associated strains whose sequences were available from GenBank. All three of the strong inhibitors of CoNS were most closely related to *Corynebacterium propinquum*, while the weak inhibitors of CoNS were closely related to either *Corynebacterium pseudodiphtheriticum* (5 isolates) or "*Corynebacterium genitalium*" (1 isolate), which is currently not a recognized *Corynebacterium* species name (37) (Fig. S1). For clarity, we refer to the *Corynebacterium* strong inhibitors of CoNS as *C. propinquum* and the other isolates as *C. genitalium* or *C. pseudodiphtheriticum*. We note that all three *C. propinquum* isolates were obtained from the same individual and may represent replicate isolates instead of distinct strains (Table S1).

Iron acquisition genes are associated with increased CoNS inhibition. To identify differences among the *Corynebacterium* species strains that corresponded to differential CoNS inhibition, we took a comparative genomics approach. We generated draft genome sequences for each of the 10 *Corynebacterium* species isolates. Using the OMA algorithm, we predicted orthologs across the 10 genomes. In total, we predicted 2,702 ortholog groups, with 1,198 groups (44% total) universally shared across the 10 *Corynebacterium* species strains and 1,504 ortholog groups (56% total) that were absent in at least one strain. In particular, the gene content in *C. genitalium* HSID17239 was more divergent than those of the other isolates (Fig. 2A). Indeed, when *C. genitalium* HSID17239 was excluded from the analysis, 1,801 of the 2,702 (67% total) ortholog groups were shared universally across the remaining nine strains. Of the 2,702 ortholog groups, 1,106 were predicted to encode hypothetical or putative proteins, while the remaining 1,596 groups were annotated with functions (Table S2). There were 337 ortholog groups (12% of the total ortholog groups) that were uniquely shared among *C. propinquum* isolates (Fig. 2A). Although 223 of the orthologs were annotated as encoding hypothetical or putative proteins, a manual investigation of the 114 annotated orthologs revealed that 31 (27.2% of the subset) were annotated with functions related to iron acquisition and/or siderophore biosynthesis (Table S2). This result represents a 6.4-fold enrichment over the 4.3% abundance (68/1,596 orthologs) of the corresponding terms in all 10 *Corynebacterium* genomes (expected, 4.9%; $P = 1.3e-19$ [by a hypergeometric test]). As a second test, we identified Kyoto Encyclopedia of Genes and Genomes (KEGG) orthology (KO) terms that were enriched in *C. propinquum* genomes relative all 10 *Corynebacterium* species genomes. We annotated 169 of the
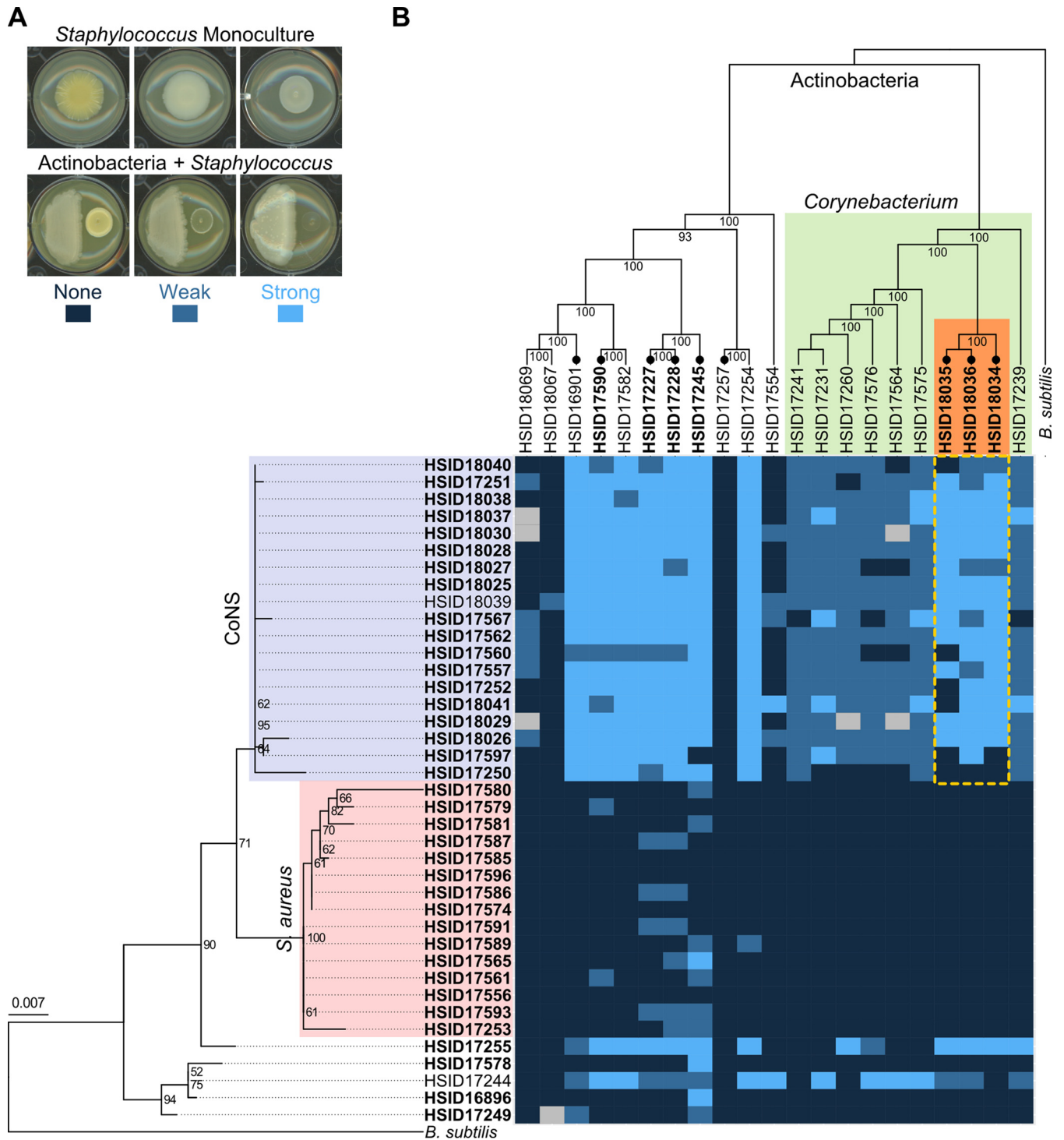
FIG 1 Inhibition of nasal *Staphylococcus* spp. by nasal *Actinobacteria*. (A) Representative images of monocultures of *Staphylococcus* and cocultures of *Actinobacteria* (left) with *Staphylococcus* species isolates (right). The inhibition scoring system is depicted below the coculture images. (B) Twenty-one nasal *Actinobacteria* isolates (horizontal) were monocultured on BHI agar wells for 1 week before 39 *Staphylococcus* species isolates (vertical) were spotted adjacent to the *Actinobacteria* colony. The colonies were cultured together for 1 week before inhibition of the *Staphylococcus* species colony was scored. The heat map displays the inhibition scores of each *Staphylococcus* species isolate when paired with the corresponding *Actinobacteria* isolate. Each interaction was technically replicated at least twice. The gray cells indicate interactions where replicates were in disagreement or the *Actinobacteria* colony overgrew the well before *Staphylococcus* inoculation. (Left) Phylogenetic tree of *Staphylococcus* species isolates built from 685 bp of the 16S rRNA gene amplified with the universal primers 27F and 1492R. (Top) Core-genome phylogenetic tree of *Actinobacteria* built from 93 conserved, single-copy genes. Both phylogenies are rooted on *B. subtilis* 168, and nodes with ≥50% bootstrap support are indicated. The dashed yellow lines highlight strong inhibition of CoNS by one clade of *Corynebacterium* spp. Strains in boldface type are siderophore producers as measured by the CAS assay. *Actinobacteria* taxa marked with ● harbor a siderophore BGC within their genome.
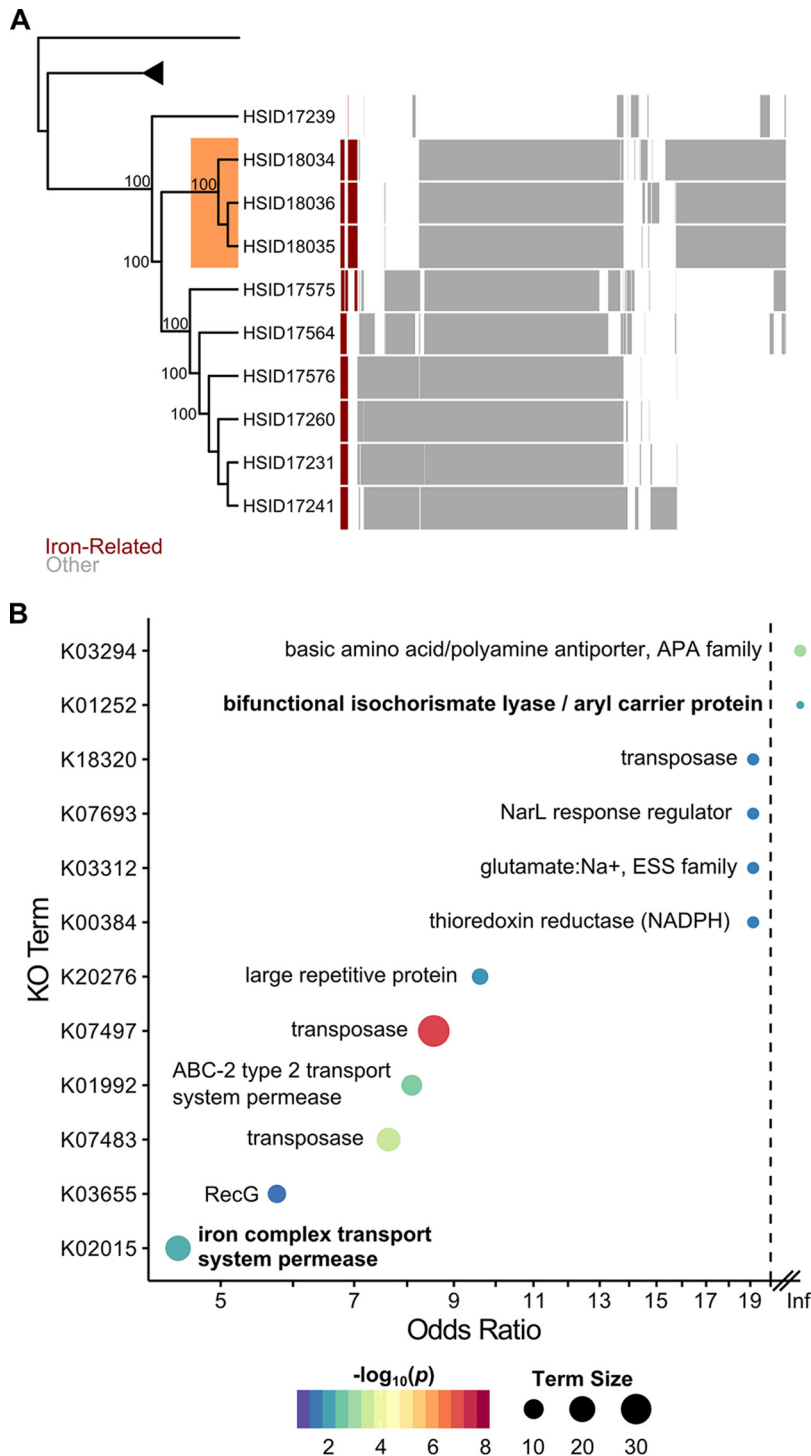
FIG 2 Comparative genomics of nasal *Corynebacterium* spp. (A, left) Core-genome phylogeny of nasal *Corynebacterium* from Fig. 1. The other *Actinobacteria* node is collapsed, as represented by a triangle. The *C. propinquum* clade is shaded in orange. (Right) Clustered presence-absence matrix of 1,504 orthologs predicted across the 10 *Corynebacterium* species genomes. The 1,198 orthologs that were conserved across all 10 genomes were excluded. Orthologs encoding functions pertaining to iron metabolism, iron transport, or siderophore biosynthesis are depicted in red. (B) KO term enrichment analysis of the orthologs uniquely shared among *C. propinquum* strains relative to all orthologs encoded within all 10 *Corynebacterium* species genomes. The odds ratios of all 12 significantly enriched ($P < 0.05$) KO terms are plotted. Note that odds ratios of infinity (Inf) correspond to KO terms where all orthologs that were annotated with the KO term were present in the enrichment set. KO terms in boldface type are related to iron transport or siderophore biosynthesis. The color of each point indicates the significance level, and the size of the point indicates how many of the orthologs were annotated with the KO term.

337 orthologs unique to *C. propinquum* (50% of the subset) with 117 KO terms. Compared to the total set of 357 KO terms, the 169 orthologs were enriched in 12 KO terms. In particular, we noted that among the KO terms, 2 KO terms were associated with iron acquisition and siderophore biosynthesis: (i) iron complex transport system permeases and (ii) bifunctional isochorismate lyase/aryl carrier proteins (Fig. 2B).

Corynebacterium propinquum produces a siderophore. The results of the gene and KO term enrichment analyses (Fig. 2) led us to hypothesize that the observed variation in inhibition of CoNS by *Corynebacterium* spp. (Fig. 1B) may be due to siderophore production. To directly detect siderophore production, we used the chrome azurol S (CAS) assay, which detects siderophore production as a color change from blue to yellow because siderophores are able to remove iron from the CAS dye complex (38). Consistent with our previous results, we confirmed siderophore production by all three *C. propinquum* strains, whereas none of the six *C. pseudodiphtheriticum* isolates or the single *C. genitalium* isolate produced detectable siderophore activity (Fig. 3A and Table S1).

Iron supplementation rescues CoNS from inhibition by *C. propinquum*. The results from the CAS assay (Fig. 3A) indicated that siderophore production is correlated with strong inhibition of CoNS. To directly test if iron sequestration by *C. propinquum* was responsible for CoNS inhibition, we repeated the coculture plate inhibition assays on brain heart infusion (BHI) medium and on BHI medium supplemented with 200 μM FeCl$_3$. We found that iron supplementation rescued CoNS from inhibition by *C. propinquum*, and non-siderophore producers were unable to inhibit CoNS under the conditions of this assay (Fig. 3B). We performed the assay with 2 *C. propinquum* siderophore producers and 5 non-siderophore producers (*C. genitalium* HSID17239 and 4 strains of *C. pseudodiphtheriticum*) against 22 strains of CoNS isolated from different nasal specimens. There were significant differences among the four experimental groups ($\chi^2 = 291.16$; $df = 3$; $P < 2.2e{-}16$ [by a Kruskal-Wallis test]), and *post hoc* analysis using Dunn's pairwise comparisons indicated that the inhibition of CoNS by *C. propinquum* on normal BHI medium was significantly increased relative to that under all other conditions ($P < 1.0e{-}40$) (Fig. 3C). This result indicates that inhibition of CoNS *in vitro* by *C. propinquum* is likely due to iron sequestration. Alternatively, iron supplementation may alter the transcription profile and repress the production an alternative factor produced by *C. propinquum* that inhibits the growth of CoNS independent of siderophore production.

The *C. propinquum*-produced siderophore is dehydroxynocardamine. As a first step to identify the siderophore produced by *C. propinquum*, we used antiSMASH to identify BGCs for siderophore biosynthesis in the *Corynebacterium* species genomes that we sequenced for this study. We identified a single 12,553-bp siderophore BGC that was present within all three *C. propinquum* genomes but absent in *C. genitalium* HSID17239 and all six *C. pseudodiphtheriticum* genomes. The *C. propinquum* siderophore BGC is comprised of seven open reading frames (ORFs), which were annotated with functions consistent with iron acquisition and siderophore biosynthesis (39–41) (Fig. 4A). Specifically, in addition to transport-associated genes, this BGC encodes a pyridoxal phosphate (PLP)-dependent decarboxylase (*dnoB*), an L-lysine N^6-monooxygenase (*dnoC*), and a siderophore synthetase (*dnoD*) that contains acyl-CoA *N*-acyltransferase (InterPro accession no. IPR016181 [http://www.ebi.ac.uk/interpro/entry/IPR016181]), aerobactin siderophore biosynthesis, IucA/IucC, N-terminal (InterPro accession no. IPR007310 [http://www.ebi.ac.uk/interpro/entry/IPR007310]), and ferric iron reductase FhuF (InterPro accession no. IPR022770 [http://www.ebi.ac.uk/interpro/entry/IPR022770]) domains. Although there were no experimentally characterized BGCs that were identical to the *C. propinquum* siderophore BGC, the order of the biosynthetic genes was identical to that of the desferrioxamine E *dfo* BGC from *Pantoea agglomerans* strain B025670 (MIBiG accession no. BGC0001572 [https://mibig.secondarymetabolites.org/repository/BGC0001572/index.html]). The biosynthesis enzymes encoded by both siderophore BGCs are highly similar (Table 1), and both synthetases belong to the type
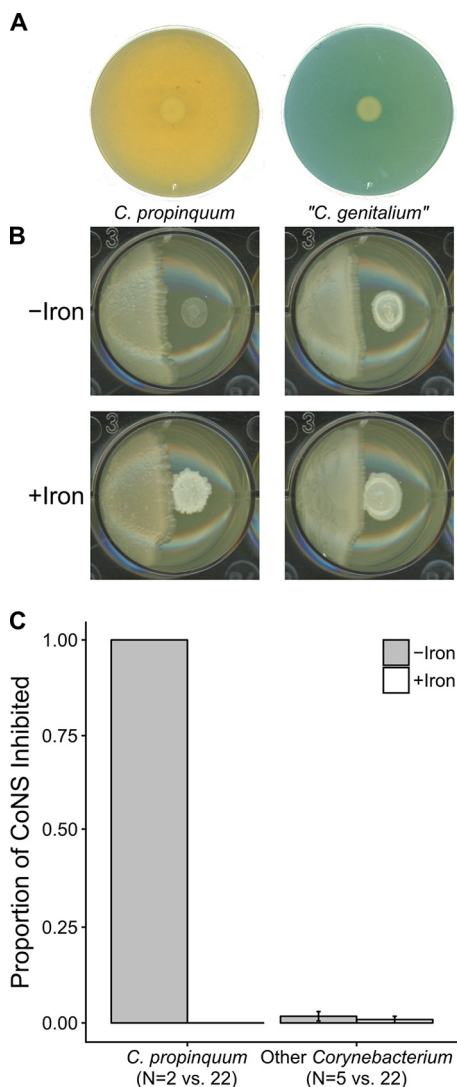
FIG 3 Siderophore production by *C. propinquum* inhibits CoNS. (A) CAS assay results from *C. propinquum* HSID18034 (left) and *C. genitalium* HSID17239 (right), which strongly and weakly inhibit CoNS, respectively. A shift in the color of the CAS overlay from blue to yellow indicates siderophore production. (B) Coculture plate inhibition between the strains in panel A and CoNS on BHI medium (−Iron) and BHI medium supplemented with 200 μM FeCl$_3$ (+Iron). (C) Coculture plate inhibition assays with *C. propinquum* (HSID18034 and HSID18036) and 5 *Corynebacterium* species non-siderophore producers (HSID17231, HSID17239, HSID17260, HSID17564, and HSID17575) against 22 CoNS strains on BHI medium (−Iron) and BHI medium supplemented with 200 μM FeCl$_3$ (+Iron). Each pairing was duplicated with consistent results. The error bars represent the standard errors of the means. The photographs in panels A and B are representative of results for duplicate samples.

C′ nonribosomal peptide synthetase-independent family (40, 41), which indicated that the siderophore produced by *C. propinquum* is likely macrocyclic.

To identify the siderophore produced by *C. propinquum*, we used comparative mass spectrometry-based metabolomics. We cultured *C. propinquum* HSID18034 and *C. genitalium* HSID17239 on BHI agar plates. We sampled agar cores near the bacterial colonies, which we extracted using methanol and analyzed using data-dependent liquid chromatography-tandem mass spectrometry (LC-MS/MS). To visualize differences in the metabolomic profiles of the two strains, we used mass spectral molecular networking (42). Surprisingly, in a network containing 222 clusters and 1,531 singletons (Fig. 4B and Fig. S3), we observed only a single cluster that was unique to *C. propinquum* HSID18034 (Fig. 4C). The central node in this cluster corresponded to *m/z* 585.358 [M + H]$^+$ (C$_{27}$H$_{48}$N$_6$O$_8$, Δppm = 3.44). The molecular weight and tandem mass
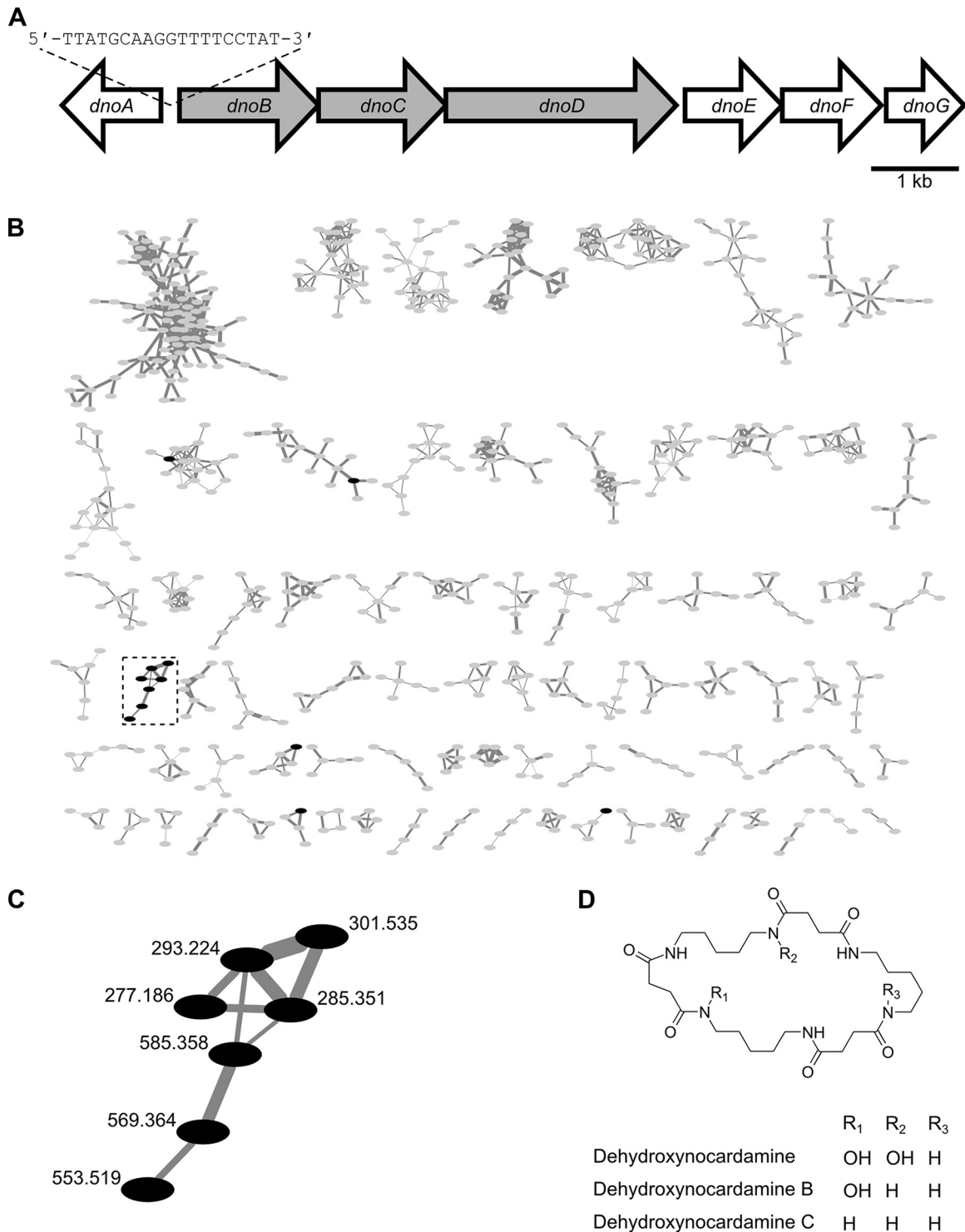
FIG 4 *Corynebacterium propinquum* produces the siderophore dehydroxynocardamine. (A) The dehydroxynocardamine BGC from *C. propinquum*. ORFs encoding biosynthetic and transport-related functions are filled with gray and white, respectively. See Table 1 for specific ORF annotation. The DtxR sequence motif is shown upstream of *dnoB*. (B) Subset of the molecular network of *C. propinquum* HSID18034 and *C. genitalium* HSID17239 agar core extracts. Gray nodes are metabolites shared by both strains, and black nodes are metabolites unique to *C. propinquum*. There were no detected metabolites that were unique to *C. genitalium*. The edges are weighted to the cosine score between the two features. A single cluster unique to *C. propinquum* is outlined in a dashed box. See Fig. S2 in the supplemental material for the full molecular network. (C) Zoomed-in view of the single cluster unique to *C. propinquum* with the nodes labeled by their corresponding *m/z*. This cluster contains single- and double-charged states of dehydroxynocardamine, dehydroxynocardamine B, and dehydroxynocardamine C. (D) Structures of dehydroxynocardamine, dehydroxynocardamine B, and dehydroxynocardamine C.

TABLE 1 *Corynebacterium propinquum* siderophore BGC annotations[a]

ORF	Size (nt)	KO term	Annotation	Desferrioxamine E BGC homolog (E value[b])
dnoA	1,074	02016	Iron siderophore ABC transporter substrate-binding protein	NA
dnoB	1,539	13745	PLP-dependent decarboxylase	*dfoJ* (4e−116)
dnoC	1,152	03897	L-Lysine N^6-monooxygenase	*dfoA* (1e−119)
dnoD	2,553	NA	Siderophore biosynthetic enzyme	*dfoC* (2e−153)
dnoE	1,062	02015	Ferric siderophore ABC transporter permease	NA
donF	1,110	02015	Siderophore ABC transport system permease	NA
dnoG	840	02013	Siderophore transport system ATP-binding protein	NA

[a]nt, nucleotides; NA, not applicable.
[b]E value from blastp protein sequence alignment.

spectrometry fragmentation pattern matched those of the siderophore dehydroxyno-cardamine (*m/z* 585.361 [M + H]$^+$, $C_{27}H_{49}N_6O_8$), which is also called terragine E (Fig. 4D). Dehydroxynocardamine has been previously reported from marine sponge-associated *Streptomyces* spp. (43) and produced by the heterologous expression of soil DNA libraries in *Streptomyces lividans* (44) but has not been reported from *Corynebacterium* spp. or any other human-associated bacteria. The other nodes in the cluster correspond to two dehydroxynocardamine analogs with protonated ions of *m/z* 569.364 [M + H]$^+$ and 553.368 [M + H]$^+$ as well as the doubly charged states of each molecule (Fig. 4C). The high similarity in fragmentation patterns as well as the differences of *m/z* −16 and −32 suggest that these compounds contained one and two fewer N-hydroxy groups than dehydroxynocardamine, respectively (Fig. 4D and Fig. S3). Furthermore, through manual investigation of the mass spectra, we identified *m/z* 312.6592 [M + Fe + H]$^{2+}$, corresponding to iron-bound dehydroxynocardamine B, indicating that dehydroxynocardamine functions as a siderophore. This parental mass was absent from the molecular network as its abundance was below the threshold for fragmentation. Based on the product, we chose to name the *C. propinquum* sidero-phore BGC *dno*, for dehydroxynocardamine.

The *dno* BGC is strongly associated with *C. propinquum*. To determine if other *Corynebacterium* spp. contain the *dno* BGC, we searched all available *Corynebacterium* species proteins in the NCBI nonredundant protein sequence (nr) database for the siderophore synthetase DnoD. We identified 17 hits in the nr database corresponding to 27 *Corynebacterium* species genome sequences. When we searched these genomes, we found that all seven ORFs of the *dno* BGC were contained by all four *C. propinquum* strains with deposited genomes, but the full *dno* BGC was not contained by any other *Corynebacterium* genome (Fig. S4A and B).

Next, we searched external naris metagenomes from 93 subjects in the Human Microbiome Project (HMP) WGS-PP1 (WGS production phase I) to determine if other nasal bacteria contain the *dno* BGC. We identified 258 contigs from a total of 718,888 contigs (0.04% total) that harbored at least one out of seven ORFs from the *dno* BGC. Of these 258 contigs, only three contigs from 2/93 total human subjects harbored all seven ORFs (Fig. S4C and D). These three contigs (lengths of 13,073, 97,360, and 178,113 bp) aligned to the *C. propinquum* HSID18034 genome with ≥98% sequence identity and ≥95% total sequence coverage, which suggests that these contigs were from *C. propinquum*. Together, these genomic and metagenomic searches indicate a strong phylogenetic signal for the association of *C. propinquum* with the *dno* BGC among *Corynebacterium* spp.

The dehydroxynocardamine BGC is expressed *in vivo*. We identified a 19-bp putative diphtheria toxin repressor (DtxR) iron box operator sequence (5′-TTATGCAA GGTTTTCCTAT-3′) (45) situated upstream of *dnoB* (Fig. 4A). When iron is abundant, DtxR forms a complex with ferrous iron and binds iron box operator sequences to repress the transcription of downstream genes, but this repression is relieved when iron is scarce (46). Transcriptional profiling of *S. aureus* from the nasal cavity indicated that bacteria colonizing the nose are iron starved *in vivo* (47). Therefore, we wanted to determine if
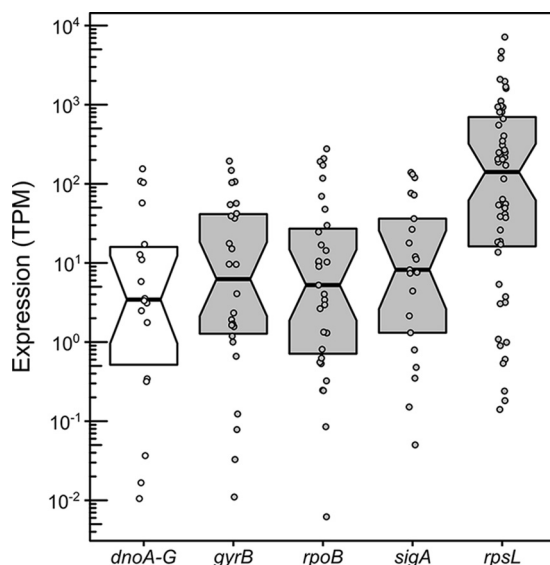
FIG 5 The dehydroxynocardamine BGC is expressed *in vivo*. Ninety-five nasal metatranscriptomes from 16 subjects in the NIH HMP were pseudoaligned to the genome of *C. propinquum* HSID18034 to detect the expression of the dehydroxynocardamine BGC (*dnoA-G*) (white) and the housekeeping genes *gyrB*, *rpoB*, *sigA*, and *rpsL* (gray). The upper and lower bounds of the notched box plot indicate the 75th and 25th percentiles, respectively. The bars indicate the medians, and the notches represent the 95% confidence intervals of the medians. Each point indicates the expression of a single gene from a metatranscriptome in transcripts per kilobase per million (TPM).

C. propinquum strains express the *dno* BGC *in vivo*. As part of the HMP prediabetes study (48), nasal swabs from the anterior nares were collected from 16 adult individuals over multiple visits and processed for metatranscriptome sequencing. We analyzed these metatranscriptomes for the expression of the *dno* BGC and several housekeeping genes (*rpoB*, *gyrB*, *sigA*, and *rpsL*). We detected *dno* expression in 7/16 individuals from at least one visit (mean, 2.5 visits/subject; median, 1 visit/subject), with expression values ranging from 0.01 to 154.69 transcripts per kilobase per million (TPM) (mean, 26.94 TPM; median, 3.44 TPM). For comparison, we detected the expression of housekeeping genes at similar levels (Fig. 5), with the exception of *rpsL*, which is known to be more highly expressed than the other selected housekeeping genes in the model Gram-positive organism *Bacillus subtilis* (49). Together, these results indicate that the dehydroxynocardamine BGC is likely expressed *in vivo*.

DISCUSSION

In this study, we investigated inhibition of nasal *Staphylococcus* species isolates by strains of sympatric *Actinobacteria*. We uncovered two distinct patterns of interactions: (i) CoNS were significantly more sensitive than *S. aureus* to inhibition by nasal *Actinobacteria*, and (ii) there was variability among *Corynebacterium* spp. in their ability to inhibit the growth of CoNS (Fig. 1). Specifically, we noted that *C. propinquum* more strongly inhibited CoNS than did other *Corynebacterium* spp. Through a combination of comparative genomics (Fig. 2) and culture-based approaches (Fig. 3), we determined that the difference in inhibitory ability was due to the production of a siderophore, dehydroxynocardamine (Fig. 4). By analyzing metatranscriptome samples from the anterior nares of human subjects, we established that the *dno* BGC is expressed *in vivo* (Fig. 5), indicating that iron-mediated exploitation competition is potentially relevant to competition and organismal fitness within the human nasal cavity.

One broad explanation for the difference in inhibition patterns between *S. aureus* and CoNS isolates that we observed (Fig. 1B) is that CoNS lack the same mechanisms that *S. aureus* uses to obtain iron from the hosts and from the external environment. For instance, CoNS strains do not grow well on iron-limited media (19) and, unlike *S. aureus*, are able to scavenge iron from human transferrin (50). Our finding that iron supple-

mentation rescues CoNS from inhibition by *C. propinquum* (Fig. 3B and C) is consistent with previous results showing that CoNS are sensitive to inhibition by desferrioxamine siderophores and other iron-chelating agents *in vitro* (51, 52). Notably, strains of both *S. aureus* and CoNS are known to produce their own carboxylate siderophores, called staphyloferrins A (53) and B (54). Using the CAS assay, we determined that all 15 isolates of *S. aureus* and nearly every CoNS isolate (30/33 tested) used in this study produced siderophores when grown in monoculture (Fig. 1B; see also Table S1 in the supplemental material). However, it is known that CoNS have markedly lower levels of siderophore production than *S. aureus* (55). Furthermore, siderophore production by CoNS is under different regulatory control than in *S. aureus* (55), which may contribute to the increased susceptibility of CoNS to iron limitation imposed by *C. propinquum*. In addition, it was previously reported that *Staphylococcus* spp. are able to use catecholate and hydroxamate siderophores produced by *Corynebacterium* spp. and other organisms (56). Perhaps, in addition to higher levels of siderophore production, *S. aureus* is also better able to pirate dehydroxynocardamine produced by *C. propinquum* and circumvent inhibition. Further work is required to determine the exact mechanism that *S. aureus* uses to survive competition with *C. propinquum* compared to CoNS.

Here, we note that siderophore-mediated inhibition does not fully explain the patterns of inhibition of CoNS by nasal *Actinobacteria*. In addition to the 3 siderophore-producing *C. propinquum* strains, only 6 of the 11 other *Actinobacteria* contained siderophore BGCs in their genomes (Fig. 1B). Furthermore, while the genomes of *Curtobacterium* sp. strain HSID17257 and *Kocuria* sp. strain HSID16901 contain siderophore BGCs, these strains did not produce siderophores (Fig. 1B and Table S1). Regardless, the latter strain strongly inhibited CoNS under our assay conditions (Fig. 1B). Together, these data indicate that nasal *Actinobacteria* likely use multiple types of mechanisms to inhibit the growth of CoNS. Perhaps these *Actinobacteria* engage in interference competition mediated by antibiotic production, which is common among nasal bacteria (30–32), to inhibit the growth of CoNS. Subsequent work will be required to identify the molecules responsible for inhibition of CoNS that are produced by non-siderophore-producing nasal *Actinobacteria*.

Exploitation competition mediated by siderophore production is common among soil and marine bacteria (57–59), but within the context of host-associated systems, siderophore production is considered a pathogen virulence factor (reviewed in reference 60) because mutants that are unable to produce siderophores are often defective in colonizing hosts and causing disease (61, 62). The view of siderophores solely as pathogen-produced molecules is strengthened by lipocalin-2, a protein component of the innate immune response that binds to catechol siderophores to prevent their uptake by bacteria and whose production is induced by bacterial colonization of mucosal surfaces (23, 24). However, thus far, little work has considered siderophore-mediated competition among the members of the microbiota and between the microbiota and pathogenic bacteria (63). For instance, siderophore piracy is reported to occur between pathogens and beneficial or commensal bacteria in the human gastrointestinal tract (64, 65), but no such mechanisms within the human nasal cavity have hitherto been reported.

In conclusion, as (i) dehydroxynocardamine is not a known virulence factor, (ii) *C. propinquum* is considered a normal part of the nasal microbiota (33, 66, 67), and (iii) the expression of *dnoA* to *dnoG* (*dnoA-G*) was detected *in vivo*, we suggest that *C. propinquum* may produce dehydroxynocardamine as a means to mediate exploitation competition for iron with other bacteria within the human nasal cavity.

MATERIALS AND METHODS

Nasal lavage specimen collection. The nasal lavage samples that we used in this study were banked as part of the COAST study (35). Informed consent was obtained from parents, and the Human Subjects Committee at the University of Wisconsin—Madison approved the study (institutional review board [IRB] approval number H-2013-1044). Briefly, lavage samples were collected by spraying Deep Sea nasal spray (Major) into one of the participant's nostrils. To collect the sample, the participant was then instructed to blow their nose into a plastic bag. Subsequently, the samples were stored at 4°C. Approximately 3 ml

of either phosphate-buffered saline or Amies transport medium (Copan Diagnostics) was added to each sample before storage at −80°C.

Strain isolation and maintenance. For general strain propagation, we used brain heart infusion (BHI) medium (DOT Scientific). All plates were solidified using 1.5% agar (VWR). For iron supplementation experiments, we added 200 μM FeCl$_3$ to the BHI agar after autoclaving and cooling the medium to 55°C before pouring the plates. Bacterial strains used in this study are listed in Table S1 in the supplemental material. To culture bacteria from the lavage samples, we spread 100 μl of each of the thawed samples onto BHI plates and incubated the plates aerobically at 37°C for 1 week. We selected ≥2 colonies of each distinct morphotype per plate and passaged the isolates aerobically on BHI plates at 37°C until we obtained pure cultures. All bacterial isolates were cryopreserved at −80°C in 25% glycerol.

Bacterial isolate identification. To identify bacterial isolates, we sequenced the 16S rRNA gene. We used colony PCR with the universal 27F (5′-AGAGTTTGATCMTGGCTCAG-3′) and 1492R (5′-CGGTTACCT TGTTACGACTT-3′) primers to amplify the 16S rRNA gene (68). We sequenced PCR products using the Sanger method at the University of Wisconsin—Madison Biotechnology Center. We identified isolates to the genus level using the Ribosomal Database Project Classifier (69). To distinguish between *S. aureus* and CoNS (e.g., *Staphylococcus capitis*, *Staphylococcus caprae*, *S. epidermidis*, and *Staphylococcus saccharolyticus*) isolates, we used BLAST searches against the NCBI 16S rRNA sequence database with a threshold sequence identity of 99%. We corroborated the identity of *Staphylococcus* species isolates using colony pigmentation and hemolysis phenotypes (70–72).

16S rRNA gene phylogenetic analysis. We aligned the 16S rRNA gene sequences using SINA (v1.2.11) (73) through the Silva Web server (74) and discarded unaligned bases at the ends of the sequences. For phylogenetic analysis, we imported the alignments into MEGA7 (75). We inferred phylogenetic trees using the maximum likelihood method based on the general time-reversible (GTR) model with 100 bootstraps. All nucleotide positions containing gaps were removed in the final analysis.

Coculture plate inhibition assays. We used coculture plate inhibition assays to assess the activity of *Actinobacteria* isolates against *Staphylococcus*. We spread *Actinobacteria* from saturated overnight-grown cultures in BHI broth over one half of a well (diameter, 2.4 cm) containing 3 ml of BHI agar on a 12-well plate (Greiner Bio-One). We incubated the plates for 1 week at 37°C. Subsequently, we spotted ~3 μl of a 10-fold-diluted saturated overnight-grown culture of each *Staphylococcus* species isolate in BHI medium adjacent to the *Actinobacteria* and returned the plates to the 37°C incubator. After 1 week of coculture, we removed the plates, scanned them, and scored the inhibition for each interaction pair. All interactions were tested with ≥2 replicates, with consistent results. An inhibition score of 0 indicated no inhibition, a score of 1 indicated weak inhibition, and a score of 2 indicated strong inhibition (Fig. 1A).

Whole-genome sequencing and assembly. We cultured bacterial strains for whole-genome sequencing in 3 ml of BHI broth supplemented with 0.5% glycine overnight at 37°C. We harvested the cells by centrifuging the cultures at 21,330 × *g* for 5 min. The cell pellets were washed with 10.3% sucrose and resuspended in 450 μl of a lysozyme solution (3 mg/ml lysozyme [Sigma], 0.3 M sucrose, 25 mM Tris-HCl [pH 8], 25 mM EDTA [pH 8]) for 30 min at 37°C. Subsequently, 13 μl of 20 mg/ml proteinase K (Thermo Fisher) was added to each sample, with additional incubation at 42°C for 15 min. Cells were lysed by adding 250 μl of 2% SDS and rocking the mixture for 15 min. DNA was purified using standard phenol-chloroform extraction and precipitated with 3 M sodium acetate and isopropanol. We visually assessed the quality of genomic DNA preparations by running samples on 0.5% Tris-borate-EDTA (TBE) gels. Genomic libraries for Illumina MiSeq 2- by 150-bp paired-end sequencing were prepared and sequenced by the University of Wisconsin—Madison Biotechnology Center. Raw reads were corrected with MUSKET v1.1 (76), and paired ends were merged with FLASH v1.2.7 (77). Reads were assembled into draft genome sequences with SPAdes v3.11.0 (78).

Core-genome phylogeny. We constructed a core-genome phylogenetic tree of nasal *Actinobacteria* as previously described (79). Briefly, we called genes in each genome using prodigal v2.6.0 (80) and used profile hidden Markov models in HMMER v3.1b2 (81) to search each genome for 93 full-length TIGRFAM amino acid sequences in the "core bacterial protein" set (GenProp0799). Each protein family was aligned using MAFFT v7.245 (82) and converted to codon alignments. We used RAxML v8.1.24 (83) to generate phylogenetic trees for each of the 93 codon alignments under the GTR gamma substitution model with 100 bootstraps. To generate the species phylogenetic tree, we used ASTRAL-II (84) from the individual phylogenetic trees with 100 bootstraps. We used FigTree v1.4.3 (http://tree.bio.ed.ac.uk/software/figtree/) to root the phylogeny on *B. subtilis* 168 and display the branch length based on proportional length to the root.

Comparative genomics. We annotated the assembled genomes using prokka v1.13 (85). For comparative genomics, we identified orthologs from the nucleotide sequences of each protein-coding open reading frame (ORF) with OMA v2.2.0 (86). To annotate orthologs with KEGG orthology (KO) terms, we used DIAMOND v0.9.21.122 (87) to query one sequence of each ortholog group against a custom database of KEGG-annotated protein sequences with an E value threshold cutoff of 1.0e−10. Each ORF was assigned the KO terms from the top BLAST hit. For KEGG KO term enrichment analysis, we used the GSEABase v1.42.0 package (88) and GOstats v1.7.4 (89) in R and performed a hypergeometric test with a *P* value cutoff of 0.05.

Identification of BGCs. To identify BGCs, we used antiSMASH 4.0.2 (90). Proteins from all identified BGCs were aligned via all-versus-all DIAMOND (query coverage, >75%; percent identity, >60%). BGCs that shared over 75% of proteins were called the same family. BGC families correlated with inhibition were identified through their presence in the strong-inhibition strains and absence in the weak-inhibition strains. Proteins from all identified BGCs were combined with all proteins from MIBiG v1.3 (91) and

subsequently aligned with DIAMOND with the same parameters as the ones listed above to identify biosynthetic gene similarities to previously described BGCs.

Chrome azurol S assay. We used the overlay chrome azurol S (CAS) assay to test for siderophore production as previously described (92). We cultured *Corynebacterium* spp. overnight in 3 ml BHI medium at 37°C. We diluted the cultures grown overnight to an optical density at 600 nm (OD_{600}) of 2 and spotted 5 μl onto 10-ml BHI agar plates (diameter, 5 cm). We incubated the plates at 37°C for 4 days to ensure robust *Corynebacterium* growth. Subsequently, we overlaid each plate with 6 ml of CAS reagent overlay [100 μM CAS, 200 μM hexadecyltrimethylammonium bromide, 10 μM $FeCl_3 \cdot 6H_2O$, 10 mM piperazine-N,N'-bis(2-ethanesulfonic acid) (PIPES) (pH 6.8), 1% agarose] (38, 92) and incubated the plates at ambient temperature in the dark overnight before scanning plates for a color change from blue to yellow, indicating the production of a siderophore (38).

Siderophore identification and mass spectral molecular networking. To identify the siderophore, we used comparative mass spectrometry. We spotted 10 μl of either *C. genitalium* HSID17231 or *C. propinquum* HSID18034 cultures grown overnight onto the center of 25-ml BHI agar plates (diameter, 8.5 cm). After incubating the plates as described above, we removed agar cores (diameter, 0.6 cm) from an area near the *Corynebacterium* colony using the wide end of a P1000 pipette tip. We verified siderophore activity by directly placing an agar core onto CAS assay plates and observing the color change from blue to yellow. We washed a duplicate agar core in 2 ml of 50% methanol and 2 ml of 100% methanol, which we combined and dried with a gentle air stream under reduced pressure.

Data-dependent LC-MS/MS was performed on a Thermo Scientific Q Exactive Orbitrap instrument by the University of Wisconsin Analytical Instrumentation Center of the School of Pharmacy. The liquid chromatography method was performed on a Phenomenex XB C_{18}, 2.1- by 100-mm, 2.6-μm-particle-size column with solvent A (water with 0.1% formic acid) and solvent B (acetonitrile with 0.1% formic acid). A gradient of 5% solvent B for 0.5 min to 30% solvent B over 16 min and then 97% solvent B for 2 min with a flow rate of 0.35 ml/min was used to separate the metabolites. We exported the files in mzXML format and uploaded them to Global Natural Products Social Molecular Networking (GNPS) (93). The data were filtered by removing all MS/MS peaks within ±17 Da of the precursor *m/z*. The MS/MS spectra were window filtered by choosing the top 6 peaks in the ±50-Da window throughout the spectrum. The data were clustered with MS-Cluster using a parent mass tolerance of 2.0 Da and an MS/MS fragment ion tolerance of 0.5 Da to create consensus spectra. Consensus spectra containing <2 spectra were discarded. A network was created where edges were filtered with a cosine score of >0.6 and more than 3 matched peaks. Edges between two nodes were kept in the network if each of the nodes appeared in the respective top 10 most similar nodes. The spectra in the network were then searched against GNPS spectral libraries. The library spectra were filtered in the same manner as the input data. All matches kept between network spectra and library spectra were required to have a score of >0.6 and at least 3 matched peaks. Analog search was enabled against the library, with a maximum mass shift of 100.0 Da.

Identification of the dehydroxynocardamine BGC in external naris metagenomes. We downloaded assembled metagenomes from the National Institutes of Health (NIH) Integrative Human Microbiome Project (iHMP) from the Human Microbiome Project Data Portal (https://portal.hmpdacc.org) using hmp_client. DNA was isolated from each of the 93 subjects between 1 and 3 times for a total of 227 external naris metagenomes (mean, 1.3/subject; median, 1/subject). We used the assembled metagenomes as a query against the amino acid sequences of each of the seven ORFs in the dehydroxynocardamine BGC using DIAMOND blastx (query coverage, $\geq90\%$; percent identity, $\geq40\%$).

Metatranscriptome analysis for dehydroxynocardamine BGC expression. As part of the iHMP, RNA from the anterior nares of 16 prediabetic subjects was isolated and depleted of 16S and 23S rRNAs. The RNA was converted to cDNA with random primers and paired-end sequenced using an Illumina platform (48). We downloaded the raw reads using hmp_client, as described above. We removed Illumina adapter sequences, low-quality reads, and unpaired reads using trimmomatic v0.36 (94) with the following parameter: SLIDINGWINDOW:5:20. RNA was isolated from each of the 16 subjects between 1 and 11 times for a total of 95 nasal metatranscriptomes (mean, 5.9/subject; median, 6.5/subject). For our analyses, we treated each individual metatranscriptome as a single sample. To determine the expression of the *dno* BGC, we used kallisto v0.44.0 (95) and pseudoaligned each of the metatranscriptomes onto the indexed ORFs of the *C. propinquum* HSID18034 genome. We chose to align the reads onto this genome because our genomic and metagenomic surveys (see Fig. S4 in the supplemental material) indicated that no other *Corynebacterium* species or nasal cavity-associated strain possessed the *dno* BGC. We extracted the expression data for the combined dehydroxynocardamine BGC (*dnoA-G*) and four housekeeping genes: *rpoB*, *gyrB*, *sigA*, and *rpsL*. We removed genes with <1 estimated count from the data set for a total of 148 expression counts (18 siderophore BGCs and 130 housekeeping genes).

Data availability. The genome sequences of *Actinobacteria* generated during this study have been deposited in the National Center for Biotechnology Information database under BioProject accession number PRJNA492917.

SUPPLEMENTAL MATERIAL

Supplemental material for this article may be found at https://doi.org/10.1128/AEM .02406-18.

SUPPLEMENTAL FILE 1, PDF file, 1.4 MB.
SUPPLEMENTAL FILE 2, CSV file, 0.1 MB.

ACKNOWLEDGMENTS

REFERENCES

1. Cantarel BL, Lombard V, Henrissat B. 2012. Complex carbohydrate utilization by the healthy human microbiome. PLoS One 7:e28742. https://doi.org/10.1371/journal.pone.0028742.

2. Nieuwdorp M, Gilijamse PW, Pai N, Kaplan LM. 2014. Role of the microbiome in energy regulation and metabolism. Gastroenterology 146:1525–1533. https://doi.org/10.1053/j.gastro.2014.02.008.

3. Hill MJ. 1997. Intestinal flora and endogenous vitamin synthesis. Eur J Cancer Prev 6:S43–S45. https://doi.org/10.1097/00008469-199703001-00009.

4. Resta SC. 2009. Effects of probiotics and commensals on intestinal epithelial physiology: implications for nutrient handling. J Physiol 587:4169–4174. https://doi.org/10.1113/jphysiol.2009.176370.

5. Buffie CG, Pamer EG. 2013. Microbiota-mediated colonization resistance against intestinal pathogens. Nat Rev Immunol 13:790–801. https://doi.org/10.1038/nri3535.

6. Schubert AM, Sinani H, Schloss PD. 2015. Antibiotic-induced alterations of the murine gut microbiota and subsequent effects on colonization resistance against Clostridium difficile. mBio 6:e00974-15. https://doi.org/10.1128/mBio.00974-15.

7. Siegel SJ, Weiser JN. 2015. Mechanisms of bacterial colonization of the respiratory tract. Annu Rev Microbiol 69:425–444. https://doi.org/10.1146/annurev-micro-091014-104209.

8. Brown SA, Palmer KL, Whiteley M. 2008. Revisiting the host as a growth medium. Nat Rev Microbiol 6:657–666. https://doi.org/10.1038/nrmicro1955.

9. Fuchs TM, Eisenreich W, Heesemann J, Goebel W. 2012. Metabolic adaptation of human pathogenic and related nonpathogenic bacteria to extra- and intracellular habitats. FEMS Microbiol Rev 36:435–462. https://doi.org/10.1111/j.1574-6976.2011.00301.x.

10. Koropatkin NM, Cameron EA, Martens EC. 2012. How glycan metabolism shapes the human gut microbiota. Nat Rev Microbiol 10:323–335. https://doi.org/10.1038/nrmicro2746.

11. Berry D, Stecher B, Schintlmeister A, Reichert J, Brugiroux S, Wild B, Wanek W, Richter A, Rauch I, Decker T, Loy A, Wagner M. 2013. Host-compound foraging by intestinal microbiota revealed by single-cell stable isotope probing. Proc Natl Acad Sci U S A 110:4720–4725. https://doi.org/10.1073/pnas.1219247110.

12. Winter SE, Thiennimitr P, Winter MG, Butler BP, Huseby DL, Crawford RW, Russell JM, Bevins CL, Adams LG, Tsolis RM, Roth JR, Bäumler AJ. 2010. Gut inflammation provides a respiratory electron acceptor for Salmonella. Nature 467:426–429. https://doi.org/10.1038/nature09415.

13. Whiteside JA, Voss JG. 1973. Incidence and lipolytic activity of Propionibacterium acnes (Corynebacterium acnes group I) and P. granulosum (C. acnes group II) in acne and in normal skin. J Invest Dermatol 60:94–97. https://doi.org/10.1111/1523-1747.ep12724177.

14. Miskin JE, Farrell AM, Cunliffe WJ, Holland KT. 1997. Propionibacterium acnes, a resident of lipid-rich human skin, produces a 33 kDa extracellular lipase encoded by gehA. Microbiology 143:1745–1755. https://doi.org/10.1099/00221287-143-5-1745.

15. Rebillo T, Hawk JL. 1978. Skin surface glycerol levels in acne vulgaris. J Invest Dermatol 70:352–354. https://doi.org/10.1111/1523-1747.ep12543549.

16. Flynn JM, Niccum D, Dunitz JM, Hunter RC. 2016. Evidence and role for bacterial mucin degradation in cystic fibrosis airway disease. PLoS Pathog 12:e1005846. https://doi.org/10.1371/journal.ppat.1005846.

17. Lorin MI, Gaerlan PF, Mandel ID. 1972. Quantitative composition of nasal secretions in normal subjects. J Lab Clin Med 80:275–281.

18. Vanthanouvong V, Roomans GM. 2004. Methods for determining the composition of nasal fluid by X-ray microanalysis. Microsc Res Tech 63:122–128. https://doi.org/10.1002/jemt.20020.

19. Krismer B, Liebeke M, Janek D, Nega M, Rautenberg M, Hornig G, Unger C, Weidenmaier C, Lalk M, Peschel A. 2014. Nutrient limitation governs Staphylococcus aureus metabolism and niche adaptation in the human nose. PLoS Pathog 10:e1003862. https://doi.org/10.1371/journal.ppat.1003862.

20. Ferraris RP, Yasharpour S, Lloyd KC, Mirzayan R, Diamond JM. 1990. Luminal glucose concentrations in the gut under normal conditions. Am J Physiol 259:G822–G837. https://doi.org/10.1152/ajpgi.1990.259.5.G822.

21. Pezzulo AA, Gutiérrez J, Duschner KS, McConnell KS, Taft PJ, Ernst SE, Yahr TL, Rahmouni K, Klesney-Tait J, Stoltz DA, Zabner J. 2011. Glucose depletion in the airway surface liquid is essential for sterility of the airways. PLoS One 6:e16166. https://doi.org/10.1371/journal.pone.0016166.

22. Winkelmann G. 2002. Microbial siderophore-mediated transport. Biochem Soc Trans 30:691–696. https://doi.org/10.1042/bst0300691.

23. Nelson AL, Barasch JM, Bunte RM, Weiser JN. 2005. Bacterial colonization of nasal mucosa induces expression of siderocalin, an iron-sequestering component of innate immunity. Cell Microbiol 7:1404–1417. https://doi.org/10.1111/j.1462-5822.2005.00566.x.

24. Bachman MA, Miller VL, Weiser JN. 2009. Mucosal lipocalin 2 has proinflammatory and iron-sequestering effects in response to bacterial enterobactin. PLoS Pathog 5:e1000622. https://doi.org/10.1371/journal.ppat.1000622.

25. Cosgrove K, Coutts G, Jonsson I-M, Tarkowski A, Kokai-Kun JF, Mond JJ, Foster SJ. 2007. Catalase (KatA) and alkyl hydroperoxide reductase (AhpC) have compensatory roles in peroxide stress resistance and are required for survival, persistence, and nasal colonization in Staphylococcus aureus. J Bacteriol 189:1025–1035. https://doi.org/10.1128/JB.01524-06.

26. Hoopman TC, Liu W, Joslin SN, Pybus C, Sedillo JL, Labandeira-Rey M, Laurence CA, Wang W, Richardson JA, Bakaletz LO, Hansen EJ. 2012. Use of the chinchilla model for nasopharyngeal colonization to study gene expression by Moraxella catarrhalis. Infect Immun 80:982–995. https://doi.org/10.1128/IAI.05918-11.

27. Hibbing ME, Fuqua C, Parsek MR, Peterson SB. 2010. Bacterial

competition: surviving and thriving in the microbial jungle. Nat Rev Microbiol 8:15–25. https://doi.org/10.1038/nrmicro2259.

28. Stubbendieck RM, Vargas-Bautista C, Straight PD. 2016. Bacterial communities: interactions to scale. Front Microbiol 7:1234. https://doi.org/10.3389/fmicb.2016.01234.

29. Stubbendieck RM, Straight PD. 2016. Multifaceted interfaces of bacterial competition. J Bacteriol 198:2145–2155. https://doi.org/10.1128/JB.00275-16.

30. Zipperer A, Konnerth MC, Laux C, Berscheid A, Janek D, Weidenmaier C, Burian M, Schilling NA, Slavetinsky C, Marschal M, Willmann M, Kalbacher H, Schittek B, Brötz-Oesterhelt H, Grond S, Peschel A, Krismer B. 2016. Human commensals producing a novel antibiotic impair pathogen colonization. Nature 535:511–516. https://doi.org/10.1038/nature18634.

31. Bomar L, Brugger SD, Yost BH, Davies SS, Lemon KP. 2016. Corynebacterium accolens releases antipneumococcal free fatty acids from human nostril and skin surface triacylglycerols. mBio 7:e01725-15. https://doi.org/10.1128/mBio.01725-15.

32. Janek D, Zipperer A, Kulik A, Krismer B, Peschel A. 2016. High frequency and diversity of antimicrobial activities produced by nasal Staphylococcus strains against bacterial competitors. PLoS Pathog 12:e1005812. https://doi.org/10.1371/journal.ppat.1005812.

33. Brugger SD, Bomar L, Lemon KP. 2016. Commensal-pathogen interactions along the human nasal passages. PLoS Pathog 12:e1005633. https://doi.org/10.1371/journal.ppat.1005633.

34. Bomar L, Brugger SD, Lemon KP. 2018. Bacterial microbiota of the nasal passages across the span of human life. Curr Opin Microbiol 41:8–14. https://doi.org/10.1016/j.mib.2017.10.023.

35. Lemanske RF. 2002. The childhood origins of asthma (COAST) study. Pediatr Allergy Immunol 13:38–43. https://doi.org/10.1034/j.1399-3038.13.s.15.8.x.

36. Stoltz DJ, Jackson DJ, Evans MD, Gangnon RE, Tisler CJ, Gern JE, Lemanske RF. 2013. Specific patterns of allergic sensitization in early childhood and asthma & rhinitis risk. Clin Exp Allergy 43:233–241. https://doi.org/10.1111/cea.12050.

37. Whitman WB, Goodfellow M, Kämpfer P, Busse H-J, Trujillo ME, Ludwig W, Suzuki K-I, Parte A (ed). 2012. Bergey's manual of systematic bacteriology, 2nd ed, vol 5. The Actinobacteria. Springer, New York, NY.

38. Schwyn B, Neilands JB. 1987. Universal chemical assay for the detection and determination of siderophores. Anal Biochem 160:47–56. https://doi.org/10.1016/0003-2697(87)90612-9.

39. Bosello M, Mielcarek A, Giessen TW, Marahiel MA. 2012. An enzymatic pathway for the biosynthesis of the formylhydroxyornithine required for rhodochelin iron coordination. Biochemistry 51:3059–3066. https://doi.org/10.1021/bi201837f.

40. Oves-Costales D, Kadi N, Challis GL. 2009. The long-overlooked enzymology of a nonribosomal peptide synthetase-independent pathway for virulence-conferring siderophore biosynthesis. Chem Commun (Camb) 2009:6530–6541. https://doi.org/10.1039/b913092f.

41. Carroll CS, Moore MM. 2018. Ironing out siderophore biosynthesis: a review of non-ribosomal peptide synthetase (NRPS)-independent siderophore synthetases. Crit Rev Biochem Mol Biol 53:356–381. https://doi.org/10.1080/10409238.2018.1476449.

42. Guthals A, Watrous JD, Dorrestein PC, Bandeira N. 2012. The spectral networks paradigm in high throughput mass spectrometry. Mol Biosyst 8:2535–2544. https://doi.org/10.1039/c2mb25085c.

43. Lee HS, Hee JS, Kyoung HJ, Tae SK, Oh KB, Shin J. 2005. Cyclic peptides of the nocardamine class from a marine-derived bacterium of the genus Streptomyces. J Nat Prod 68:623–625. https://doi.org/10.1021/np040220g.

44. Wang GYS, Graziani E, Waters B, Pan W, Li X, McDermott J, Meurer G, Saxena G, Andersen RJ, Davies J. 2000. Novel natural products from soil DNA libraries in a streptomycete host. Org Lett 2:2401–2404. https://doi.org/10.1021/ol005860z.

45. Lee JH, Wang T, Ault K, Liu J, Schmitt MP, Holmes RK. 1997. Identification and characterization of three new promoter/operators from Corynebacterium diphtheriae that are regulated by the diphtheria toxin repressor (DtxR) and iron. Infect Immun 65:4273–4280.

46. Kunkle CA, Schmitt MP. 2005. Analysis of a DtxR-regulated iron transport and siderophore biosynthesis gene cluster in Corynebacterium diphtheriae. J Bacteriol 187:422–433. https://doi.org/10.1128/JB.187.2.422-433.2005.

47. Chaves-Moreno D, Wos-Oxley ML, Jáuregui R, Medina E, Oxley AP, Pieper DH. 2016. Exploring the transcriptome of Staphylococcus aureus in its natural niche. Sci Rep 6:33174. https://doi.org/10.1038/srep33174.

48. Integrative HMP Research Network Consortium. 2014. The Integrative Human Microbiome Project: dynamic analysis of microbiome-host omics profiles during periods of human health and disease. Cell Host Microbe 16:276–289. https://doi.org/10.1016/j.chom.2014.08.014.

49. Zhu B, Stülke J. 2018. SubtiWiki in 2018: from genes and proteins to functional network annotation of the model organism Bacillus subtilis. Nucleic Acids Res 46:D743–D748. https://doi.org/10.1093/nar/gkx908.

50. Lindsay JA, Riley TV, Mee BJ. 1995. Staphylococcus aureus but not Staphylococcus epidermidis can acquire iron from transferrin. Microbiology 141:197–203. https://doi.org/10.1099/00221287-141-1-197.

51. Lindsay JA, Riley TV. 1991. Susceptibility to desferrioxamine: a new test for the identification of Staphylococcus epidermidis. J Med Microbiol 35:45–48. https://doi.org/10.1099/00222615-35-1-45.

52. Heuck D, Witte W, Braulke C, Reissbrodt R. 1994. Susceptibility to desferrioxamines and other chelators of coagulase-negative staphylococci. Zentralbl Bakteriol 280:304–311. https://doi.org/10.1016/S0934-8840(11)80591-8.

53. Cotton JL, Tao J, Balibar CJ. 2009. Identification and characterization of the Staphylococcus aureus gene cluster coding for staphyloferrin A. Biochemistry 48:1025–1035. https://doi.org/10.1021/bi801844c.

54. Cheung J, Beasley FC, Liu S, Lajoie GA, Heinrichs DE. 2009. Molecular characterization of staphyloferrin B biosynthesis in Staphylococcus aureus. Mol Microbiol 74:594–608. https://doi.org/10.1111/j.1365-2958.2009.06880.x.

55. Lindsay JA, Riley TV. 1994. Staphylococcal iron requirements, siderophore production, and iron-regulated protein expression. Infect Immun 62:2309–2314.

56. Szarapińska-Kwaszewska J, Mikucki J. 1997. Utilization of Staphylococcus siderophores produced by Corynebacterium and coryneform bacteria. Med Dosw Mikrobiol 49:131–140. (In Polish.)

57. Traxler MF, Seyedsayamdost MR, Clardy J, Kolter R. 2012. Interspecies modulation of bacterial development through iron competition and siderophore piracy. Mol Microbiol 86:628–644. https://doi.org/10.1111/mmi.12008.

58. Galet J, Deveau A, Hôtel L, Frey-Klett P, Leblond P, Aigle B. 2015. Pseudomonas fluorescens pirates both ferrioxamine and ferricoelichelin siderophores from Streptomyces ambofaciens. Appl Environ Microbiol 81:3132–3141. https://doi.org/10.1128/AEM.03520-14.

59. Patin NV, Duncan KR, Dorrestein PC, Jensen PR. 2016. Competitive strategies differentiate closely related species of marine actinobacteria. ISME J 10:478–490. https://doi.org/10.1038/ismej.2015.128.

60. Holden VI, Bachman MA. 2015. Diverging roles of bacterial siderophores during infection. Metallomics 7:986–995. https://doi.org/10.1039/c4mt00333k.

61. Register KB, Ducey TF, Brockmeier SL, Dyer DW. 2001. Reduced virulence of a Bordetella bronchiseptica siderophore mutant in neonatal swine. Infect Immun 69:2137–2143. https://doi.org/10.1128/IAI.69.4.2137-2143.2001.

62. Fetherston JD, Kirillina O, Bobrov AG, Paulley JT, Perry RD. 2010. The yersiniabactin transport system is critical for the pathogenesis of bubonic and pneumonic plague. Infect Immun 78:2045–2052. https://doi.org/10.1128/IAI.01236-09.

63. Barber MF, Elde NC. 2015. Buried treasure: evolutionary perspectives on microbial iron piracy. Trends Genet 31:627–636. https://doi.org/10.1016/j.tig.2015.09.001.

64. Naikare H, Butcher J, Flint A, Xu J, Raymond KN, Stintzi A. 2013. Campylobacter jejuni ferric-enterobactin receptor CfrA is TonB3 dependent and mediates iron acquisition from structurally different catechol siderophores. Metallomics 5:988–996. https://doi.org/10.1039/c3mt20254b.

65. Deriu E, Liu JZ, Pezeshki M, Edwards RA, Ochoa RJ, Contreras H, Libby SJ, Fang FC, Raffatellu M. 2013. Probiotic bacteria reduce Salmonella Typhimurium intestinal colonization by competing for iron. Cell Host Microbe 14:26–37. https://doi.org/10.1016/j.chom.2013.06.007.

66. Schenck LP, Surette MG, Bowdish DME. 2016. Composition and immunological significance of the upper respiratory tract microbiota. FEBS Lett 590:3705–3720. https://doi.org/10.1002/1873-3468.12455.

67. Teutsch B, Berger A, Marosevic D, Schönberger K, Lâm T-T, Hubert K, Beer S, Wienert P, Ackermann N, Claus H, Drayß M, Thiel K, van der Linden M, Vogel U, Sing A. 2017. Corynebacterium species nasopharyngeal carriage in asymptomatic individuals aged ≥ 65 years in Germany. Infection 45:607–611. https://doi.org/10.1007/s15010-017-1017-0.

68. Frank JA, Reich CI, Sharma S, Weisbaum JS, Wilson BA, Olsen GJ. 2008. Critical evaluation of two primers commonly used for amplification of

bacterial 16S rRNA genes. Appl Environ Microbiol 74:2461–2470. https://doi.org/10.1128/AEM.02272-07.

69. Wang Q, Garrity GM, Tiedje JM, Cole JR. 2007. Naive Bayesian classifier for rapid assignment of rRNA sequences into the new bacterial taxonomy. Appl Environ Microbiol 73:5261–5267. https://doi.org/10.1128/AEM.00062-07.

70. Kloos WE, Schleifer KH. 1975. Isolation and characterization of staphylococci from human skin. II. Descriptions of four new species: Staphylococcus warneri, Staphylococcus capitis, Staphylococcus hominis, and Staphylococcus simulans. Int J Syst Bacteriol 25:62–79. https://doi.org/10.1099/00207713-25-1-62.

71. Foster T. 1996. Staphylococcus, chapter 12. In Baron S (ed), Medical microbiology, 4th ed. University of Texas Medical Branch at Galveston, Galveston, TX.

72. Namvar AE, Bastarahang S, Abbasi N, Ghehi GS, Farhadbakhtiarian S, Arezi P, Hosseini M, Baravati SZ, Jokar Z, Chermahin SG. 2014. Clinical characteristics of Staphylococcus epidermidis: a systematic review. GMS Hyg Infect Control 9:Doc23. https://doi.org/10.3205/dgkh000243.

73. Pruesse E, Peplies J, Glöckner FO. 2012. SINA: accurate high-throughput multiple sequence alignment of ribosomal RNA genes. Bioinformatics 28:1823–1829. https://doi.org/10.1093/bioinformatics/bts252.

74. Quast C, Pruesse E, Yilmaz P, Gerken J, Schweer T, Yarza P, Peplies J, Glöckner FO. 2013. The SILVA ribosomal RNA gene database project: improved data processing and Web-based tools. Nucleic Acids Res 41:D590–D596. https://doi.org/10.1093/nar/gks1219.

75. Kumar S, Stecher G, Tamura K. 2016. MEGA7: Molecular Evolutionary Genetics Analysis version 7.0 for bigger datasets. Mol Biol Evol 33:1870–1874. https://doi.org/10.1093/molbev/msw054.

76. Liu Y, Schröder J, Schmidt B. 2013. Musket: a multistage k-mer spectrum-based error corrector for Illumina sequence data. Bioinformatics 29:308–315. https://doi.org/10.1093/bioinformatics/bts690.

77. Magoč T, Salzberg SL. 2011. FLASH: fast length adjustment of short reads to improve genome assemblies. Bioinformatics 27:2957–2963. https://doi.org/10.1093/bioinformatics/btr507.

78. Bankevich A, Nurk S, Antipov D, Gurevich AA, Dvorkin M, Kulikov AS, Lesin VM, Nikolenko SI, Pham S, Prjibelski AD, Pyshkin AV, Sirotkin AV, Vyahhi N, Tesler G, Alekseyev MA, Pevzner PA. 2012. SPAdes: a new genome assembly algorithm and its applications to single-cell sequencing. J Comput Biol 19:455–477. https://doi.org/10.1089/cmb.2012.0021.

79. Chevrette MG, Currie CR. 2019. Emerging evolutionary paradigms in antibiotic discovery. J Ind Microbiol Biotechnol 46:257–271. https://doi.org/10.1007/s10295-018-2085-6.

80. Hyatt D, Chen G-L, Locascio PF, Land ML, Larimer FW, Hauser LJ. 2010. Prodigal: prokaryotic gene recognition and translation initiation site identification. BMC Bioinformatics 11:119. https://doi.org/10.1186/1471-2105-11-119.

81. Eddy SR. 2011. Accelerated profile HMM searches. PLoS Comput Biol 7:e1002195. https://doi.org/10.1371/journal.pcbi.1002195.

82. Katoh K, Standley DM. 2013. MAFFT multiple sequence alignment software version 7: improvements in performance and usability. Mol Biol Evol 30:772–780. https://doi.org/10.1093/molbev/mst010.

83. Stamatakis A. 2014. RAxML version 8: a tool for phylogenetic analysis and post-analysis of large phylogenies. Bioinformatics 30:1312–1313. https://doi.org/10.1093/bioinformatics/btu033.

84. Mirarab S, Warnow T. 2015. ASTRAL-II: coalescent-based species tree estimation with many hundreds of taxa and thousands of genes. Bioinformatics 31:i44–i52. https://doi.org/10.1093/bioinformatics/btv234.

85. Seemann T. 2014. Prokka: rapid prokaryotic genome annotation. Bioinformatics 30:2068–2069. https://doi.org/10.1093/bioinformatics/btu153.

86. Train C-M, Glover NM, Gonnet GH, Altenhoff AM, Dessimoz C. 2017. Orthologous Matrix (OMA) algorithm 2.0: more robust to asymmetric evolutionary rates and more scalable hierarchical orthologous group inference. Bioinformatics 33:i75–i82. https://doi.org/10.1093/bioinformatics/btx229.

87. Buchfink B, Xie C, Huson DH. 2015. Fast and sensitive protein alignment using DIAMOND. Nat Methods 12:59–60. https://doi.org/10.1038/nmeth.3176.

88. Morgan M, Falcon S, Gentleman R. 2018. GSEABase: gene set enrichment data structures and methods. https://bioconductor.org/packages/release/bioc/html/GSEABase.html.

89. Falcon S, Gentleman R. 2007. Using GOstats to test gene lists for GO term association. Bioinformatics 23:257–258. https://doi.org/10.1093/bioinformatics/btl567.

90. Blin K, Wolf T, Chevrette MG, Lu X, Schwalen CJ, Kautsar SA, Suarez Duran HG, de Los Santos ELC, Kim HU, Nave M, Dickschat JS, Mitchell DA, Shelest E, Breitling R, Takano E, Lee SY, Weber T, Medema MH. 2017. antiSMASH 4.0—improvements in chemistry prediction and gene cluster boundary identification. Nucleic Acids Res 45:W36–W41. https://doi.org/10.1093/nar/gkx319.

91. Medema MH, Kottmann R, Yilmaz P, Cummings M, Biggins JB, Blin K, de Bruijn I, Chooi YH, Claesen J, Coates RC, Cruz-Morales P, Duddela S, Düsterhus S, Edwards DJ, Fewer DP, Garg N, Geiger C, Gomez-Escribano JP, Greule A, Hadjithomas M, Haines AS, Helfrich EJN, Hillwig ML, Ishida K, Jones AC, Jones CS, Jungmann K, Kegler C, Kim HU, Kötter P, Krug D, Masschelein J, Melnik AV, Mantovani SM, Monroe EA, Moore M, Moss N, Nützmann H-W, Pan G, Pati A, Petras D, Reen FJ, Rosconi F, Rui Z, Tian Z, Tobias NJ, Tsunematsu Y, Wiemann P, Wyckoff E, Yan X, et al. 2015. Minimum information about a biosynthetic gene cluster. Nat Chem Biol 11:625–631. https://doi.org/10.1038/nchembio.1890.

92. Pérez-Miranda S, Cabirol N, George-Téllez R, Zamudio-Rivera LS, Fernández FJ. 2007. O-CAS, a fast and universal method for siderophore detection. J Microbiol Methods 70:127–131. https://doi.org/10.1016/j.mimet.2007.03.023.

93. Wang M, Carver JJ, Phelan VV, Sanchez LM, Garg N, Peng Y, Nguyen DD, Watrous J, Kapono CA, Luzzatto-Knaan T, Porto C, Bouslimani A, Melnik AV, Meehan MJ, Liu W-T, Crüsemann M, Boudreau PD, Esquenazi E, Sandoval-Calderón M, Kersten RD, Pace LA, Quinn RA, Duncan KR, Hsu C-C, Floros DJ, Gavilan RG, Kleigrewe K, Northen T, Dutton RJ, Parrot D, Carlson EE, Aigle B, Michelsen CF, Jelsbak L, Sohlenkamp C, Pevzner P, Edlund A, McLean J, Piel J, Murphy BT, Gerwick L, Liaw C-C, Yang Y-L, Humpf H-U, Maansson M, Keyzers RA, Sims AC, Johnson AR, Sidebottom AM, Sedio BE, et al. 2016. Sharing and community curation of mass spectrometry data with Global Natural Products Social Molecular Networking. Nat Biotechnol 34:828–837. https://doi.org/10.1038/nbt.3597.

94. Bolger AM, Lohse M, Usadel B. 2014. Trimmomatic: a flexible trimmer for Illumina sequence data. Bioinformatics 30:2114–2120. https://doi.org/10.1093/bioinformatics/btu170.

95. Bray NL, Pimentel H, Melsted PP, Pachter L. 2016. Near-optimal probabilistic RNA-seq quantification. Nat Biotechnol 34:525–527. https://doi.org/10.1038/nbt.3519.